International Journal of Mass Spectrometry 444 (2019) 116179

Contents lists available at ScienceDirect

International Journal of Mass Spectrometry

journal homepage: www.elsevier.com/locate/ijms

IR ion spectroscopy in a combined approach with MS/MS and IM-MS to discriminate epimeric anthocyanin glycosides (cyanidin 3-O-glucoside and -galactoside)

Davide Corinti [a, ***], Alessandro Maccelli [a], Maria Elisa Crestoni [a], Stefania Cesa [a], Deborah Quaglio [a], Bruno Botta [a], Cinzia Ingallina [a], Luisa Mannina [a], Aura Tintaru [b], Barbara Chiavarino [a, **], Simonetta Fornarini [a, *]

[a] Dipartimento di Chimica e Tecnologie del Farmaco, Università di Roma "La Sapienza", I-00185, Roma, Italy
[b] Aix Marseille Univ, CNRS, Institut de Chimie Radicalaire, UMR 7273, 13397, Marseille, France

ARTICLE INFO

Article history:
Received 10 April 2019
Received in revised form
8 July 2019
Accepted 8 July 2019
Available online 9 July 2019

Keywords:
Antocyanidins
Structure determination
Epimer discrimination
IRMPD spectroscopy
FT-ICR mass spectrometry

ABSTRACT

Anthocyanins are widespread in plants and flowers, being responsible for their different colouring. Two representative members of this family have been selected, cyanidin 3-*O*-β-glucopyranoside and 3-*O*-β-galactopyranoside, and probed by mass spectrometry based methods, testing their performance in discriminating between the two epimers. The native anthocyanins, delivered into the gas phase by electrospray ionization, display a comparable drift time in ion mobility mass spectrometry (IM-MS) and a common fragment, corresponding to loss of the sugar moiety, in their collision induced dissociation (CID) pattern. However, the IR multiple photon dissociation (IRMPD) spectra in the fingerprint range show a feature particularly evident in the case of the glucoside. This signature is used to identify the presence of cyanidin 3-*O*-β-glucopyranoside in a natural extract of pomegranate. In an effort to increase any differentiation between the two epimers, aluminum complexes were prepared and sampled for elemental composition by FT-ICR-MS. CID experiments now display an extensive fragmentation pattern, showing few product ions peculiar to each species. More noteworthy is the IRMPD behavior in the OH stretching range showing significant differences in the spectra of the two epimers. DFT calculations allow to interpret the observed distinct bands due to a varied network of hydrogen bonding and relative conformer stability.

1. Introduction

Anthocyanins are important phytochemicals belonging to the flavonoid group, present in many plants, fruits and flowers. Typically overexpressed during rapid cell growth, these secondary metabolites play an important role for their free radical scavenging properties [1]. Chemically, they represent the polyoxygenated glycosidic derivatives of 2-phenylbenzopyrylium (flavylium) ion, depicted in Fig. 1. More than 300 different anthocyanins have been identified in nature, which are constituted by one of the twenty aglycones, conjugated with diverse sugars [2]. Among the six most common aglycones, i.e. delphinidin, cyanidin, malvidin, pelargonidin, peonidin and petunidin, cyanidin is the most widespread in nature [3]. As reported in Fig. 1, cyanidin holds hydroxyl substituents on positions 3,5,7,3′ and 4'. The enzymatic reaction performed by glucosyltransferase on the hydroxyl group on C3 position leads to the formation of cyanidin 3-glucoside [4].

The heterocyclic oxygen atom in ring C is positively charged, though the charge is distributed by resonance forms also over rings A and B so imparting pronounced acid properties to the OH groups. In fact, the flavylium cation is predominant only at low pH while prototropic equilibria favor neutral quinoidal and anionic forms at higher pH [5,6]. Furthermore, chalcone isomers and hemiketal species are also involved in pH dependent equilibria in aqueous solution [5,6]. In anthocyanidins, the flavylium core is modified by the presence of various hydroxyl and methoxyl substituents and O-

* Corresponding author.
** Corresponding author.
*** Corresponding author.
E-mail addresses: Davide.corinti@uniroma1.it (D. Corinti), Barbara.chiavarino@uniroma1.it (B. Chiavarino), simonetta.fornarini@uniroma1.it (S. Fornarini).

https://doi.org/10.1016/j.ijms.2019.116179

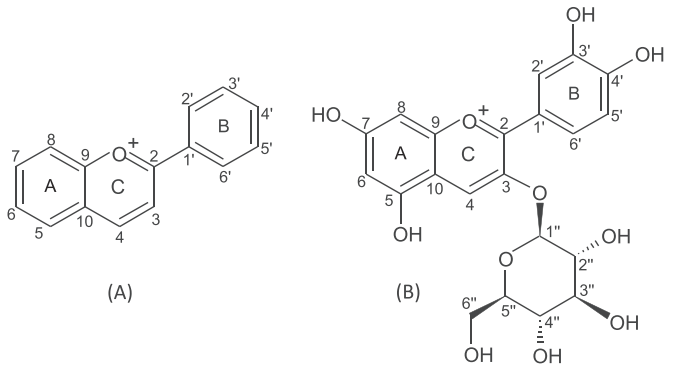

Fig. 1. Structure of flavylium ion (A) and of cyanidin 3-glucoside (B).

glycosylation considerably enhances the stability. Generally, O-glycosylation occurs in position 3 for anthocyanidin monoglycosides and in position 3 and 5 for the diglycosides. Glucose is the most common sugar of anthocyanidin glycosides, but also galactose, rhamnose, arabinose, xylose, galactose, and rutinose (6-O-L-rhamnosyl-D-glucose) can be included [7].

The anthocyanins are natural dyes, responsible for the diverse coloration of many flowers (e. g. pansies, hydrangeas, delphiniums and pelargonium) fruits and vegetables (e. g. berries, grapes, and eggplant) ranging from orange to violet. The variation in color has been ascribed to several structural and environmental factors such as the number of hydroxyl groups and degree of methylation and glycosylation, the prevalence of prototropic and pseudo base forms, self-assembly and the formation of metal complexes [4,5,8–10]. Due to the intense coloration, water solubility, and non-toxicity, anthocyanins are widely used as dyes in the food industry to replace synthetic food colorants in view of an increased usage of approved natural colors [11,12]. Cyanidin, for example, is the magenta color named E−163b. Furthermore, anthocyanins are efficient antioxidants due to their radical scavenging activity, associated to protective effects against capillary fragility, aging and inflammation [13–15]. Other potential health promoting effects have been also reported as anticancer, antidiabetic, antiviral, cardioprotective agents [16–20]. However, some controversy is reported in the literature concerning the relative contribution of anthocyanins versus the sugar-free aglycones in terms of bioavailability and bioactive potential. While first assumed that only aglycones could enter in the blood circulation, recently the absorption and metabolism of anthocyanin glycosides have been also reported [21] and both the aglycone and the glycosylate are recognized to take part to anthocyanin absorption and excretion in humans [16].

In this context, deciphering the anthocyanin profile in plant tissues and extracts is desirable in view of the potential use as food natural pigments and/or health food supplements. Several analytical and physico-chemical approaches have been previously adopted for their characterization [22]. In particular, tandem mass spectrometry (MS) has provided an invaluable contribution due to the high sensitivity, the option of coupling with liquid chromatography and the structural insight [23–27]. In this contribution, an approach based on electrospray ionization (ESI) coupled with FT-ICR mass spectrometry (FT-ICR-MS), IR multiple photon dissociation (IRMPD) spectroscopy, collision induced dissociation (CID) and ion mobility mass spectrometry (IM-MS) has been used to characterize cyanidin-3-*O*-β-glucopyranoside and 3-*O*-β-galactopyranoside (henceforth indicated as $Cy3Glu^+$ and $Cy3Gal^+$, respectively) and their aluminum(III) complexes. Metal complexation strategies have been already employed to determine structural features of flavonoid conjugates by tandem MS, because metal complexes were found to yield more information upon CID than the uncomplexed flavonoids [28–31].

In recent years IRMPD spectroscopy has become a powerful tool to interrogate molecular properties and binding interactions in a variety of (bio)molecular ions and metal adducts, including (modified) amino acids and peptides [32–37], metabolites [38–40], saccharides [41–43] nutraceuticals [44–48] and cofactors [49]. Finally, IRMPD spectroscopy has been tested in probing the metabolite present in an Italian pomegranate fruit.

2. Materials and methods

2.1. Materials and sampling by ESI

Cyanidin 3-glucoside chloride, cyanidin 3-galactoside chloride and $AlCl_3$ were research grade commercial products (Sigma-Aldrich s. r.l. Milan, Italy). An Italian pomegranate (*Punica granatum*, L.) was purchased from a local grocery store. Sampling of $Cy3Glu^+$ and $Cy3Gal^+$ was obtained by ESI of a 10 μM methanolic solution of either cyanidin 3-glucoside chloride or cyanidin 3-galactoside chloride, respectively. Aluminum complexes were obtained by mixing equimolar solutions (10 μM) of the cyanidin compound and $AlCl_3$ in methanol. Water was rather avoided as solvent to prevent hydrolysis of the anthocyanins [11,50].

2.2. High resolution FT-ICR-MS

High-resolution FT-ICR-MS analyses were carried out using a Bruker BioApex 4.7T FT-ICR mass spectrometer equipped with an Apollo I ESI source. The acquisitions were performed in positive ionization mode with an average mass resolving power, m/Δm50%, of 60000 at m/z 400 and an infusion flow rate of 120 μl h^{-1}. The raw data, acquired by the Xmass software package, were treated using the DataAnalysis program (Bruker Daltonics).

2.3. Ion mobility experiments

Traveling wave ion mobility mass spectrometry (TWIMS-MS) was performed with a Synapt G2 HDMS quadrupole/time-of-flight (Manchester, UK) equipped with an ESI source operating in positive mode. Samples were introduced at 5 μL min^{-1} flow rate (capillary voltage +2.8 kV, sampling cone voltage +30 V) under a curtain gas (N_2) flow of 100 L h^{-1} heated at 35 °C. Accurate mass experiments were performed using reference ions from CH_3COONa internal standard. Methanolic solutions of the selected sample have been directly infused. All IM-MS spectra were recorded in the 50–1200 *m*/*z* range, with trap bias DC voltage of 45 V, helium cell gas flow of 180 mL min^{-1}, and the TWIMS cell operated at 3.45 mbar of N_2 with the following wave parameters: 900 m s^{-1} wave velocity and 35 V wave heights. All data analyses were conducted using the MassLynx 4.1 and DriftScope 2.1 programs provided by Waters. The drift timescale of the TWIMS-MS experiments was converted to a collision cross-section scale, following the calibration procedure described previously [51].

2.4. IRMPD experiments

The general procedure and experimental setup for IRMPD experiments, based on the coupling of a tunable IR laser source with modified ion trap mass spectrometers, as well as for ancillary CID measurements, have been described in detail previously [52–54].

Two distinct energy ranges were considered for IRMPD experiments. To record IRMPD spectra in the fingerprint range (900-1900 cm^{-1}) the ions of interest were assayed in a hybrid FT-ICR tandem mass spectrometer (APEX-Qe Bruker) equipped with a

7.0 T actively shielded magnet, an ESI source and a quadrupole-hexapole interface, and then irradiated for 250 ms to 1 s using the beamline of a free electron laser (FEL) at the Centre Laser Infrarouge d'Orsay (CLIO) [52,53]. Ions were mass-selected in the quadrupole and accumulated in the hexapole for 0.5 s for collisional cooling with argon, prior to their transfer into the ICR cell. The electron energy of the FEL was set at 41 MeV, to achieve suitable laser power in the frequency range of interest. Vibrational modes associated with the OH stretches were examined in the 3200-3800 cm^{-1} frequency range. To this purpose, a Paul ion trap mass spectrometer (Esquire 6000+, Bruker Daltonics) coupled to an optical parametric oscillator/amplifier (OPO/OPA) laser system (LaserVision) was used as described previously [55]. In the trap, ions were accumulated for 1 ms and then mass-selected prior to IR irradiation. Post-irradiation mass spectra were recorded averaging 5 accumulations. The irradiation time was varied from 0.3 to 1 s, depending on the system. IRMPD spectra were obtained by plotting the photofragmentation yield R ($R = -\ln[I_{parent}/(I_{parent} + \Sigma I_{fragment})]$, where I_{parent} and $I_{fragment}$ represent the intensities of the mass peaks of parent and fragment ions, respectively) as a function of the wavenumber of the IR radiation [52,53].

2.5. Pomegranate sample preparation

2.5.1. Liquid–liquid extraction

From the fresh pomegranate fruit, 60 arils, corresponding to 22 g, were extracted by mechanical removal and stored at −20 °C. Arils, frozen in liquid nitrogen, were crushed using a pestle, in order to facilitate the extraction. The freshly homogenate was added with 35 mL $CH_3OH/CHCl_3$ (5:2 v/v) and continuously stirred for 1 h, according to the Bligh-Dyer extraction method [56]. The extraction was conducted at 0 °C to avoid undesired degradation of metabolites. As expected, the methanolic phase showed a characteristic reddish color indicative of a high anthocyanin content. This fraction was then clarified with a 0.45 μm pore size membrane filter to remove the microparticulate before the steps of MS analysis and solid phase extraction (SPE).

2.5.2. Solid phase extraction

An adaption of the Ferreiro-Gonzàlez method [57] has allowed to perform the SPE extraction of the anthocyanins from the Bligh-Dyer extract in a homemade apparatus. SPE is one of the most selective, fast and cheap methods to easily remove interfering components and contaminants, in order to isolate and concentrate target compounds [58]. A commercial 6 mL Supelco reversed-phase C18 cartridge was used. The flow rate was set to 1 mL min^{-1}. The column was preconditioned with 10 mL of methanol. Then, 10 mL of extract were loaded onto the cartridge and subsequently washed with 10 mL of distilled water. Finally, the adsorbed fraction was eluted with 1 mL of acidic methanol (HCl at pH = 2). The resulting solution was neutralized using ammonia and evaporated to dryness. A comprehensive extraction scheme is reported in Scheme S1 in the supplementary data (SD).

2.6. Qualitative HPLC-DAD analysis of pomegranate extracts

HPLC analyses of the pomegranate extract were performed with a PerkinElmer apparatus (Waltham, MA, USA) consisting of a Serie 200 LC pump, a Serie 200 DAD and a Serie 200 autosampler, using the Totalchrom PerkinElmer software for the data acquisition. The chromatographic separation was performed as previously described [59], with minor changes, on a Luna RP18 column (250 × 4.6 mm i. d., 5 μm) using a mobile phase made of water acidified by formic acid (5%) and acetonitrile in a linear gradient with a flow rate of 1 mL min^{-1} at 530 nm. Acetonitrile was changed from 2% to 15% in 40'.

2.7. Computational details

An exploration of the conformer distribution for plausible isomers of $Cy3Glu^+$ and $Cy3Gal^+$ was performed using the Conformer Distribution tool, as implemented in the Spartan'16 software package, together with PM6 pseudo-empirical method. Additional guess structures devised by chemical intuition. The low energy conformers were optimized at the B3LYP/6-311 + G** level of theory, using Gaussian 09 Rev D.01 [60–62]. Subsequently, the whole set of optimized geometries was submitted to harmonic vibrational frequency computations to obtain linear IR spectra and thermodynamic corrections. Low-lying selected conformers of the two isomers were re-optimized using the B3LYP-D3 functional and the same basis set mentioned above, to include the contribution of dispersion effects [63]. Harmonic vibrational frequencies and thermal corrections of the newly optimized geometries have been also calculated at this same level.

All the theoretical IR spectra presented in this work are obtained at the B3LYP/6-311 + G** level of theory. The harmonic IR frequencies have been scaled by 0.974 and 0.957 in the fingerprint region and in the O–H stretching range, respectively, in line with factors used in previous work employing the same level of theory [64,65]. A Gaussian shape with a full width at half maximum of 20 cm^{-1} in the fingerprint range and of 5 cm^{-1} in the O–H stretching range was adopted to better simulate the experimental spectrum.

3. Results and discussion

3.1. Characterization and sampling of cyanidin 3-glucoside and -galactoside

3.1.1. CID and ion mobility experiments

The discrimination between cyanidin 3-O-glucoside ($Cy3Glu^+$) and cyanidin 3-O-galactoside ($Cy3Gal^+$) is reported to be a difficult task, unless using a chromatographic separation [66,67], in particular due to the absence of characteristic fragmentation channels. Indeed, when submitted to CID, both isomers present just one product ion, the cyanidin cation at *m/z* 287 (Fig. 2), generated by the neutral loss of a dehydrated sugar moiety, as previously observed for cyanidin-3-O-glucoside and cyanidin-3,5-diglucoside [25].

The use of ion mobility is also amenable to our samples. Indeed, separation of isomeric monosaccharide methyl glycosides, such as 4-methyl-glucopyranoside, 4-methyl-galactopyranoside and 4-methylmannopyranoside, was successfully achieved using ion mobility [68,69]. However, this approach does not appear especially promising when tested on $Cy3Glu^+$ and $Cy3Gal^+$. In fact, both species show a single peak in the mobility diagram, with closely similar (though well reproducible) arrival times of 10.39 and 10.32 ms for $Cy3Glu^+$ and $Cy3Gal^+$, respectively (Fig. S1 in the SD).

3.1.2. IRMPD spectroscopy and computational assay of reference compounds

$Cy3Glu^+$ and $Cy3Gal^+$ were then assayed by IRMPD spectroscopy. Their photofragmentation is coherent with the CID experiments showing a unique product at *m/z* 287. IRMPD spectra are reported in Fig. 3 ($Cy3Glu^+$ in blue and $Cy3Gal^+$ in red) together with calculated IR spectra of selected conformers **Cy3Glu_1–3** and **Cy3Gal_1–3** (black profiles). Geometries and calculated IR spectra of other conformers for $Cy3Glu^+$ and $Cy3Gal^+$ are reported in Fig. S2 and Fig. S3, respectively. **Cy3Glu_1,2** and **Cy3Gal_1,2** are the most stable geometries found in the conformational landscape of $Cy3Glu^+$ and $Cy3Gal^+$, respectively. These structures show a $^4C_1$

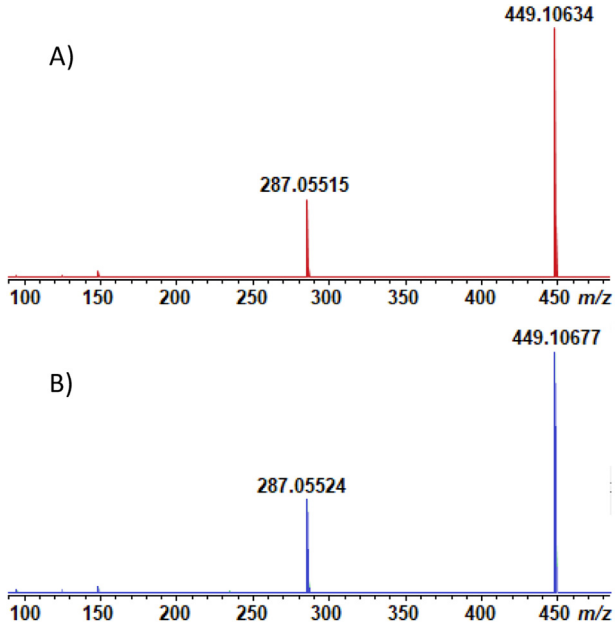

Fig. 2. CID mass spectra of A) $Cy3Glu^+$ and B) $Cy3Gal^+$. The molecular formula of the cyanidin cation fragment has been confirmed by accurate mass determination, showing 1 ppm error relative to the calculated exact mass (287.05556).

conformation regarding the sugar moiety with different orientation with respect to the aglycon part of the molecule, allowing different H-bond interactions of sugar hydroxyl groups with phenol hydroxyls. The remaining **Cy3Glu_3** and **Cy3Gal_3** species present instead a sugar $^1C_4$ conformation, which is known to be higher in energy [70,71] particularly in the case of galactose [72], as confirmed by our calculations. In fact, the free energies of **Cy3Glu_3** and **Cy3Gal_3** are 26.9 and 43.4 kJ mol^{-1}, relative to the most stable conformer. Dispersion corrected calculations [63] do not substantially modify the relative free energies of the presented structures (Fig. 3), in particular regarding **Cy3Glu_2** and **Cy3Gal_2**. However, an appreciable stabilizing effect is found on the $^1C_4$ structures, such as **Cy3Glu_3** and **Cy3Gal_3**. It may be underlined that the H-bond interactions present a similar network for $Cy3Glu^+$ and $Cy3Gal^+$ species of matching numbering.

In particular, both **Cy3Glu_1** and **Cy3Gal_1** show the same C3′OH···O(H)C6″ hydrogen bond interaction, while the secondary hydroxyl groups are all engaged in consecutive H bonds. The main difference between the two isomers lies in the equatorial conformation of the C4″ hydroxyl group in **Cy3Glu_1**, while axial in **Cy3Gal_1**. Only in the latter case is a H-bond allowed between the C4″ hydroxyl group and the primary alcohol functionality (C6"OH···O(H)C4″). Conformers **Cy3Glu_2** and **Cy3Gal_2** rather show the C5OH···O(H)C6″ hydrogen bond interaction, while the above mentioned C6"OH···O(H)C4″ hydrogen bonding is inhibited. This point accounts for the larger energy difference between **Cy3Gal_1** and **Cy3Gal_2** when compared to the **Cy3Glu_1** and **Cy3Glu_2** couple. In fact, **Cy3Glu_2** and **Cy3Gal_2** show relative free energies of 13.5 and 21.1 kJ mol^{-1}, respectively, depending on the additional stabilization of **Cy3Gal_1**.

In the IRMPD spectra of $Cy3Gal^+$ and $Cy3Glu^+$, a few elements can be highlighted comparing the experiment with the theoretical IR spectra plotted in Fig. 3. In the OH stretching range, $Cy3Glu^+$ displays one main band at 3638 cm^{-1}, in good agreement with the vibrational frequencies of the unperturbed resorcinol OH stretches, calculated at ca. 3650 cm^{-1} for all displayed structures. A weaker signal at 3566 cm^{-1} may be assigned to the stretching of the catechol OH involved in H bonding with the ortho hydroxyl group, which is calculated at 3566 cm^{-1} for **Cy3Glu_1**. The same vibrational mode is at 3588 cm^{-1} for **Cy3Glu_2**, possibly accounting for a weak feature at 3601 cm^{-1}. In the fingerprint region, the experimental spectrum of $Cy3Glu^+$ shows several signals between 1400 and 1700 cm^{-1} due to C—C stretches coupled with CH and OH bending modes of the aglycon moiety which are conserved, with only minor differences, in the series of conformers **Cy3Glu_1**–**3**. A pronounced band at 1333 cm^{-1} can be assigned to C2′H and C3′OH bending modes, calculated at 1332 and 1321 cm^{-1}, respectively, for **Cy3Glu_1**, while the shoulder at 1297 cm^{-1} suggests the contribution of **Cy3Glu_2**, presenting vibrational modes at 1292 and 1307 cm^{-1} due to collective bending modes of CH and OH bonds. The broad and intense IRMPD signal centered at 1177 cm^{-1} is consistent with the bending modes of the aromatic hydroxyl groups calculated around 1170 cm^{-1} for the whole set of conformers **Cy3Glu_1**–**3**. The last vibrational feature to be highlighted is at 1080 cm^{-1}. In spite of its low intensity, this band is slightly more active in the case of $Cy3Glu^+$ as will be discussed in the forthcoming section. It can be regarded as an indication of the presence of **Cy3Glu_2**, which shows two distinct bands at 1057 and 1041 cm^{-1} related to COC stretches of the glucose ring. Finally, the absence of IRMPD activity in the range below 1000 cm^{-1} does not support a significant contribution of **Cy3Glu_3** because of an otherwise expected vibrational mode at 908 cm^{-1}, related to the CO stretch of the glycosidic bond.

Inspection of the IRMPD spectrum of $Cy3Gal^+$ (red profile of Fig. 3) shows a strong similarity with the one of $Cy3Glu^+$. Also for this species it is possible to assume that predominant conformers populated in the gas-phase are **Cy3Gal_1** and **Cy3Gal_2**. Few noticeable differences between the spectra of $Cy3Glu^+$ and $Cy3Gal^+$ may be seen in the fingerprint region. The discussion of the IRMPD spectrum will therefore be devoted to understanding these differences on the basis of the theoretical results. While the main band remains at 1333 cm^{-1} in the spectra of both species, the shoulder observed at 1297 cm^{-1} in the case of $Cy3Glu^+$ is slightly red-shifted to 1287 cm^{-1} in the spectrum of $Cy3Gal^+$. This evidence suggests that **Cy3Gal_2** is less important relative to **Cy3Gal_1** in the sampled gas-phase population, at variance with a more balanced presence of **Cy3Glu_1** and **Cy3Glu_2** in the $Cy3Glu^+$ ion population. In fact, this shoulder is closer in frequency to the catechol CH bending calculated at 1275 cm^{-1} for **Cy3Gal_1**. Another difference, namely the rather insignificant absorption around 1080 cm^{-1}, suggests an only minor presence of **Cy3Gal_2**. This evidence is in line with the calculated thermodynamic data.

In the 3500-3700 cm^{-1} range one notes a remarkable difference in relative intensity between the “free” resorcinol OH stretching modes and the abnormally low band for the OH stretching of the cathecol unit. In the interpretation of IRMPD spectroscopy data using calculated linear IR spectra, frequency values are typically more informative than relative intensities [73]. However, bands associated to OH stretching modes engaged in hydrogen bonding (such as the catecholic OHs in the sampled species) often present a particularly critical case in being grossly under revealed in the experimental spectrum [74–77]. Vanishingly small intensities also appear to affect other OH stretching modes expected at lower frequencies due to involvement in strong H bonds. Below 3500 cm^{-1} signals pertaining to the saccharide unit are not observed. A plausible explanation is ascribed to hydrogen bonding being impaired as IR photons are absorbed, which removes the pertinent OH stretching from resonance, thus decreasing IRMPD yield. Other factors are likely to contribute, though, possibly including inefficient intramolecular vibrational energy redistribution.

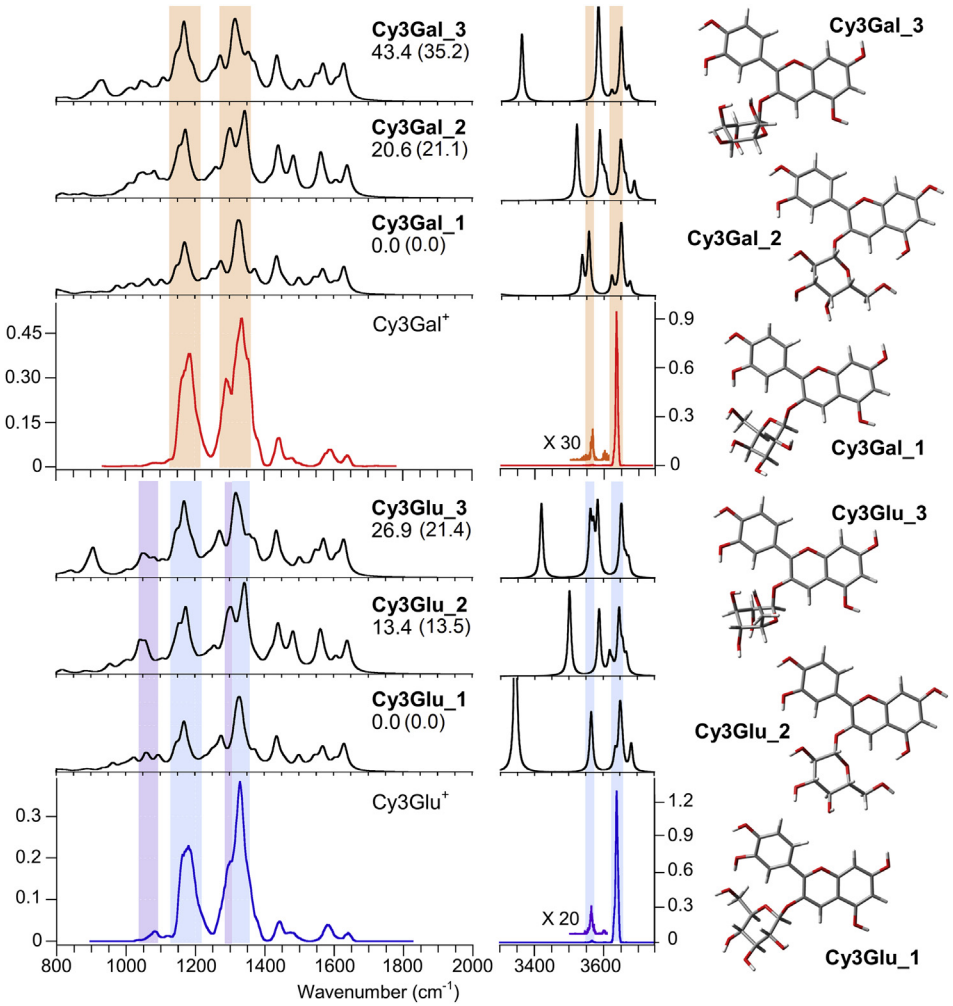

Fig. 3. IRMPD spectra of Cy3Glu$^+$ (blue profile) and Cy3Gal$^+$ (red profile) and calculated IR spectra of selected conformers **Cy3Glu_1**–**3** and **Cy3Gal_1**–**3**. Relative ΔG°(298 K) values in kJ mol^{-1} are reported at B3LYP and B3LYP-D3 (in brackets) levels. The optimized geometries at B3LYP/6-311 + G** are shown on the right. (For interpretation of the references to color in this figure legend, the reader is referred to the Web version of this article.)

3.1.3. IRMPD spectroscopy of pomegranate extract

In view of the small, but distinct, differences observed in the IRMPD spectra of the two Cy3Glu$^+$ and Cy3Gal$^+$ isomers in the fingerprint region (800-2000 cm^{-1}), IRMPD spectroscopy was performed on the ion at *m/z* 449, isolated in the quadrupole of a hybrid FT-ICR tandem mass spectrometer, from a pomegranate extract. The resulting IRMPD spectrum is shown in Fig. 4 plotted together with the IRMPD spectra of the two anthocyanin standard compounds.

When submitted to irradiation with resonant photons, the ion at *m/z* 449 yields a fragment at *m/z* 287, as reported for both Cy3Glu$^+$ and Cy3Gal$^+$. Aiming to discriminate between the two isomers, one may focus on the presence of the band at ca. 1080 cm^{-1}. As reported previously, the spectrum of Cy3Glu$^+$ (panel A of Fig. 4) presents a clearly resolved band followed by a weaker one at 1130 cm^{-1}. The same does not apply to the IRMPD spectrum of Cy3Gal$^+$. In fact, in the same region this species shows a broader and not resolved absorption of smaller intensity. The spectrum of the species isolated from the extract shows indeed a resolved vibrational feature at 1080 cm^{-1} accompanied by the smaller band at 1130 cm^{-1}, in fair agreement with the presence of a predominant if not exclusive contribution of Cy3Glu$^+$ in the extract (Fig. 4). Also the appearance of the major band at 1333 cm^{-1} and its shoulder at 1297 cm^{-1} is

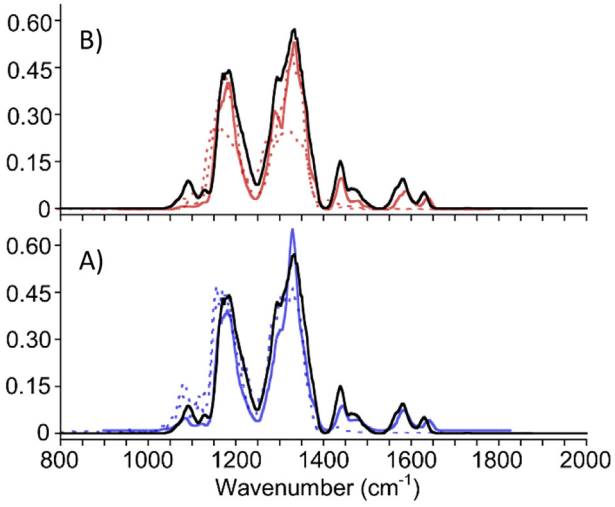

Fig. 4. IRMPD spectrum of the ion at *m/z* 449 isolated from the pomegranate extract (black profiles) plotted together with the IRMPD spectra of the standard compounds, Cy3Glu$^+$ (panel A, in blue) and Cy3Gal$^+$ (panel B, in red). Replicates of the experiment are reported with dotted lines. (For interpretation of the references to color in this figure legend, the reader is referred to the Web version of this article.)

best matched by the IRMPD spectrum of $Cy3Glu^+$. The observed vibrational features of the ion isolated from the extract appear in better agreement with the ones of $Cy3Glu^+$, thus confirming the predominant presence of the glucose-containing isomer in the pomegranate extract.

3.1.4. HPLC assay of pomegranate extract vs. reference compounds

In order to support the evidence obtained by IRMPD spectroscopy, the pomegranate extract was also analyzed by HPLC. The chromatograms reported in Fig. S4 in the SD unambiguously indicate the presence of $Cy3Glu^+$ in the complex biological mixture, verified by comparison with external standards. Moreover, delphinidin 3,5-diglucoside, cyanidin 3,5 diglucoside, and delphinidin 3-glucoside were tentatively identified by comparison with literature data [78]. Conversely, $Cy3Gal^+$, was clearly not revealed in the sample. It is already well documented that $Cy3Glu^+$ and $Cy3Gal^+$ can be discriminated by HPLC [66,67]. Therefore, the combined approaches agree on the sole presence of $Cy3Glu^+$ among the possible cyanidin monoglucosides in the present pomegranate extract.

3.2. Characterization of aluminum complexes of cyanidin 3-glucoside and −galactoside

Fig. 4 has shown a possible way to discriminate between the presence of either $Cy3Glu^+$ and $Cy3Gal^+$ using IRMPD spectroscopy in the fingerprint region. However, there are two main issues in using this approach for analytical means which have to be clarified. The former regards the instrumentation. IRMPD spectroscopy in the fingerprint region may still require the use of a FEL, in particular to appreciate small differences such as the ones highlighted in Fig. 4. Solving differences in the XH stretching range could cope with this issue, because the 3000-3800 cm^{-1} range can be accessed using tabletop OPO/OPA or dye lasers. The second problem regards the limited performance of IRMPD spectroscopy in allowing to discriminate $Cy3Glu^+$ and $Cy3Gal^+$ epimers. Making a derivative of these compounds was devised, aiming to magnify any spectroscopic difference by complexation with aluminum, known to bind anthocyanins also in nature [79–81].

3.2.1. High resolution FT-ICR-MS and CID experiments

When the anthocyanin solution is added with an aluminum chloride solution, a change in color is observed from red to blue/violet as depicted in Fig. S5, in correspondence with the formation of two main species, namely $[(Cy3Glu\text{-}3H)Al]^+$/$[(Cy3Gal\text{-}3H)Al]^+$ at *m/z* 473 and $[(Cy3Glu\text{-}2H)Al(OH)]^+$/$[(Cy3Gal\text{-}2H)Al(OH)]^+$ at *m/z* 491. As an example, the HR mass spectrum of the $Cy3Glu^+$/aluminum solution is reported in Fig. 5. As listed in Table 1, the elemental composition of observed ions is confirmed by the exact mass ($\Delta ppm < 1$) and by the $^{13}C/^{12}C$ ratio between experimental ion abundances, fitting with the calculated one (Fig. S6).

At variance with CID spectra for $Cy3Glu^+$ and $Cy3Gal^+$, the CID assay of their hydroxo-aluminum adducts gives a very extensive fragmentation pattern. The first fragmentation event for both $[(Cy3Glu\text{-}2H)Al(OH)]^+$ and $[(Cy3Gal\text{-}2H)Al(OH)]^+$ is by loss of a water molecule, yielding product ions at *m/z* 273 with an ensuing fragmentation pattern replicating the one displayed by $[(Cy3Glu\text{-}3H)Al]^+$ and $[(Cy3Gal\text{-}3H)Al]^+$ delivered by ESI. The observed product ions are listed in Table S1, together with the proposed neutral losses. The fragmentation pattern is characteristic of the CID of anthocyanidins, attributed to cross-ring cleavage of the C-ring or to a ring-opening followed by subsequent ejection of small neutral molecules [23,24,45].

The CID scheme involving subsequent loss of small neutral molecules, such as CH_2O, CO, and H_2O (Fig. 6) is very similar for both $[(Cy3Glu\text{-}2H)Al(OH)]^+$ and $[(Cy3Gal\text{-}2H)Al(OH)]^+$ complexes**.** However some differences may be underlined. E. g. the product ions at *m/z* 417, 401 and 399 are present only in the CID spectrum of $[(Cy3Glu\text{-}2H)Al(OH)]^+$ and the fragment ion at *m/z* 365 is observed only from $[(Cy3Gal\text{-}2H)Al(OH)]^+$. These peculiarities, however minor, sustain the use of aluminum complexation to distinguish the two epimers.

3.2.2. Ion mobility experiments

The mobility profile of $[(Cy3Glu\text{-}3H)Al]^+$ and $[(Cy3Gal\text{-}3H)Al]^+$ was explored in order to highlight possible differences induced by the coordination of a charge bearing site like Al(III). Results are reported in Fig. 7. Unfortunately, it was not possible to probe the mobility profile of the hydrated species $[(Cy3Glu\text{-}2H)AlOH]^+$ and $[(Cy3Gal\text{-}2H)AlOH]^+$ due to their low abundance and their ease to undergo water loss inside the TWIMS cell. The mobility profiles account for two different species with the same *m/z* ratio. In fact, a dimer of the assayed complex is generated during the ionization process in the Synapt G2-S. However, the ion mobility peaks could be assigned to either monomeric or dimeric complexes by comparing the mobility profile of the ions at *m/z* 473 with the ones recorded for the ^{13}C isotopic species at *m/z* 473.5 and 474, corresponding to the dimer and monomer, respectively. Therefore, ion

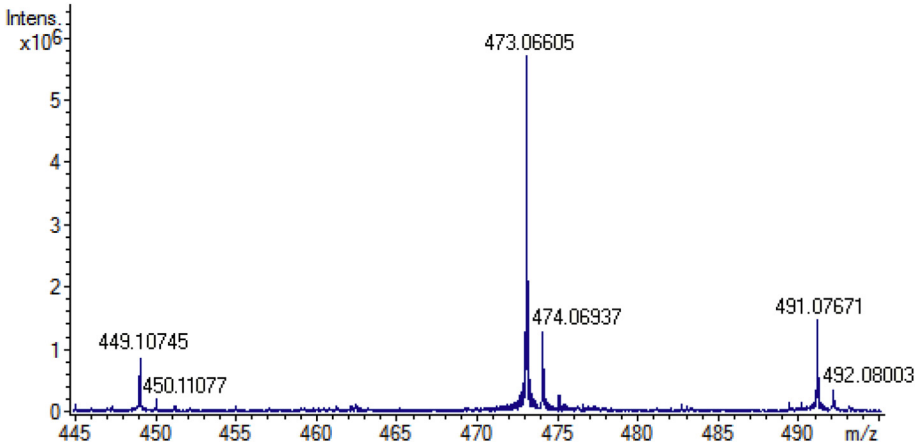

Fig. 5. FT-ICR mass spectrum of a $Cy3Glu^+$/aluminum solution. Observed ionic species are $[C_{21}H_{21}O_{11}]^+$ ($Cy3Glu^+$) at *m/z* 449.10745, $[C_{21}H_{18}O_{11}Al]^+$ ($[(Cy3Glu\text{-}3H)Al]^+$) at *m/z* 473.06605, and $[C_{21}H_{20}O_{12}Al]^+$ ($[(Cy3Glu\text{-}2H)AlOH]^+$) at 491.07671.

Table 1
High Resolution FT-ICR-MS data from a $Cy3Glu^+$/aluminum solution.

Elemental composition	Accurate mass	Exact mass	Δppm	Isotope ratio (%)[a]
$[C_{21}H_{21}O_{11}]^+$	449.10745	449.10784	−0.87	23.6 (23.4)
$[C_{21}H_{18}O_{11}Al]^+$	473.06605	473.06590	−0.31	23.0 (23.3)
$[C_{21}H_{20}O_{12}Al]^+$	491.07671	491.07645	−0.53	23.9 (23.4)

[a] The calculated $^{13}C/^{12}C$ isotopic ratio is reported in parentheses.

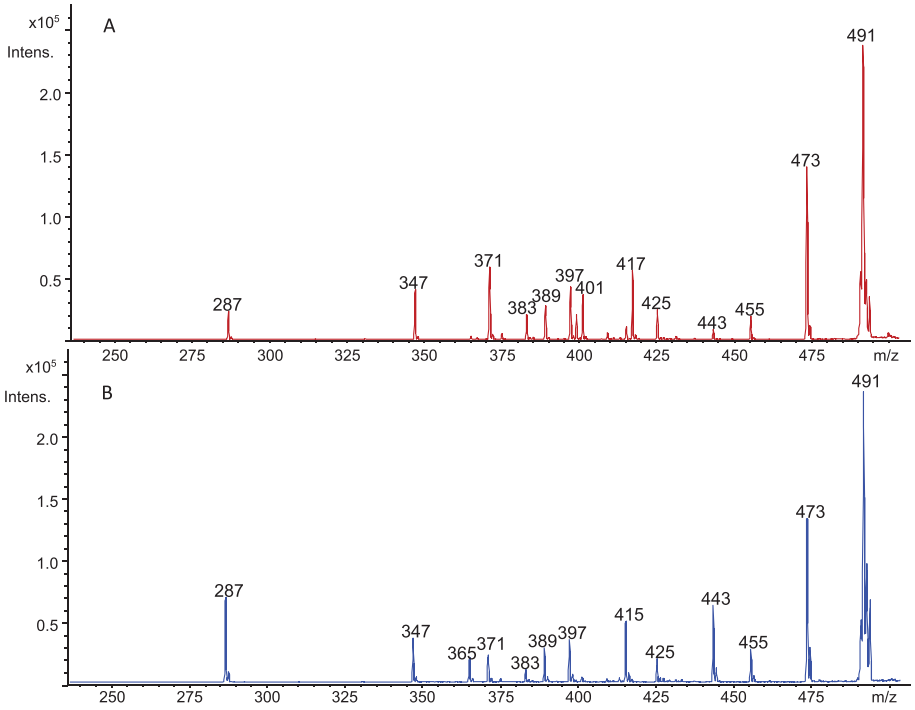

Fig. 6. CID mass spectra of $[(Cy3Glu\text{-}2H)Al(OH)]^+$ (A, red plot) and $[(Cy3Gal\text{-}2H)Al(OH)]^+$ (B, blue plot). (For interpretation of the references to color in this figure legend, the reader is referred to the Web version of this article.)

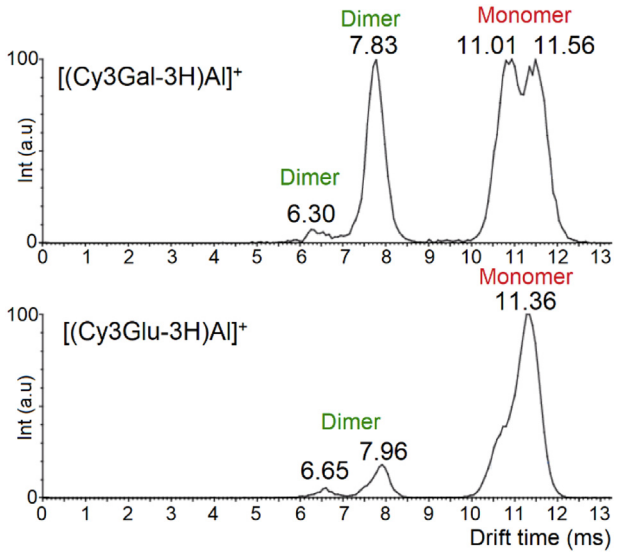

Fig. 7. Ion mobility profiles for the ions at *m/z* 449 from solutions of $Cy3Glu^+$ (bottom panel) and $Cy3Gal^+$ (top panel) in the presence of aluminum, assigned to either monomer or dimer species of $[(Cy3Glu\text{-}3H)Al]^+$ and $[(Cy3Gal\text{-}3H)Al]^+$, respectively.

mobility signals are assigned in Fig. 7, while Fig. S7 in the SD reports an enlarged mass spectrum of $[(Cy3Glu\text{-}3H)Al]^+$, showing the presence of the monomer and dimer species.

The ion mobility experiments show the presence of at least two conformers for each species. In particular, a good separation of dimer conformers is observed, while the separation of monomer complexes is not complete. In each case the two conformers (or families of conformers) should be characterized by an isomerization barrier high enough to prevent their interconversion in the TWIMS cell. One may note, however, that the interaction with aluminum has increased the diversity of the conformational space of both $Cy3Glu^+$ and $Cy3Gal^+$ because the mobility plots of the molecular cations have rather shown the presence of just a single peak (Fig. S1). However, the absolute drift time values show a rather meager difference hampering a clearcut separation of the two epimers on these grounds. Eventually, the ion mobility profile may unveil a predominant participation in an unknown sample of either $[(Cy3Glu\text{-}3H)Al]^+$ or $[(Cy3Gal\text{-}3H)Al]^+$ referring to the qualitatively different shape of the mobility profiles shown in Fig. 7.

3.2.3. Vibrational signatures of the aluminum complexes of cyanidin 3-glucoside and −galactoside

IRMPD spectra in the OH stretching range of the aluminum complexes, $[(Cy3Glu\text{-}3H)Al]^+$, $[(Cy3Gal\text{-}3H)Al]^+$, $[(Cy3Glu\text{-}2H)AlOH]^+$ and $[(Cy3Gal\text{-}2H)AlOH]^+$, are reported in Fig. 8. $[(Cy3Glu\text{-}2H)AlOH]^+$ and $[(Cy3Gal\text{-}2H)AlOH]^+$ complexes display water loss

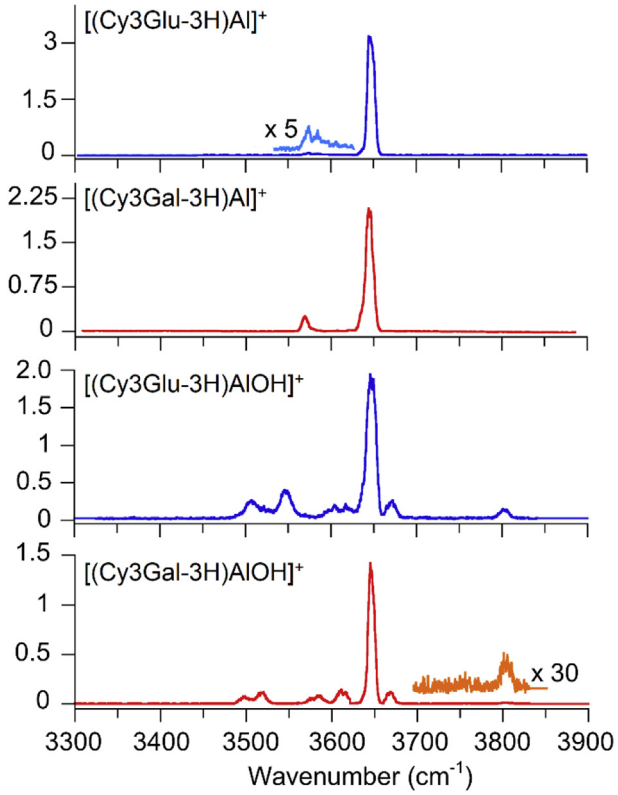

Fig. 8. IRMPD spectra of $[(Cy3Glu\text{-}3H)Al]^+$, $[(Cy3Gal\text{-}3H)Al]^+$, $[(Cy3Glu\text{-}2H)AlOH]^+$ and $[(Cy3Gal\text{-}2H)AlOH]^+$.

as unique dissociation channel on low intensity IRMPD signals. However, in correspondence of the highly active band at 3645 cm^{-1} extensive fragmentation is obtained as reported in Fig. S8 in the SD, conforming to the CID behavior shown in Fig. 6.

Comparing the four spectra in Fig. 8, the most intense IR band at 3645 cm^{-1} is conserved along the series, in agreement with its attribution to aromatic free OH stretching modes. The $[(Cy3Glu\text{-}3H)Al]^+$ and $[(Cy3Gal\text{-}3H)Al]^+$ IRMPD spectra are less informative and do not provide vibrational signatures useful for their discrimination. In contrast, the IRMPD spectra of $[(Cy3Glu\text{-}2H)AlOH]^+$ and $[(Cy3Gal\text{-}2H)AlOH]^+$ present characteristic IR absorptions, particularly in the 3450-3630 cm^{-1} spectral range. In fact, $[(Cy3Glu\text{-}2H)AlOH]^+$ shows an intense absorption at 3543 cm^{-1}, which is not observed in the IRMPD spectrum of $[(Cy3Gal\text{-}2H)AlOH]^+$, while the latter complex presents a characteristic signal at 3583 cm^{-1}. In addition, the IRMPD band at 3506 cm^{-1} of $[(Cy3Glu\text{-}2H)AlOH]^+$ is slightly red-shifted to 3497 cm^{-1} for $[(Cy3Gal\text{-}2H)AlOH]^+$ and also accompanied by a band at 3517 cm^{-1}. So, complexation with aluminum provides some signatures indicating specific structural motifs.

Fig. 9 compares the IRMPD spectrum of $[(Cy3Glu\text{-}2H)AlOH]^+$, in blue, with the calculated IR spectra of selected conformers **Cy3GluAlOH_1**, **Cy3GluAlOH_2** and **Cy3GluAlOH_3** where (HO)Al is bound to the deprotonated hydroxyl groups in C3′ and C4′ of ring B. The calculated free energies at the B3LYP level for **Cy3GluAlOH_2** and **Cy3GluAlOH_3** are 6.1 kJ mol^{-1} and 25.9 kJ mol^{-1} higher than **Cy3GluAlOH_1,** respectively. However, when dispersion is considered, **Cy3GluAlOH_3** is stabilized at a relative free energy value of 13.7 kJ mol^{-1} while **Cy3GluAlOH_2** remains at 7.4 kJ mol^{-1} (Fig. 9 in brackets). Other calculated isomers are reported in Fig. S9, including species where aluminum is chelated by the sugar moiety. The global minimum is found to be **AlOHCy3Glu_1** ($\Delta G°(298\ K) = -27.1$ kJ mol^{-1} relative to **Cy3GluAlOH_1**), a bridged structure in

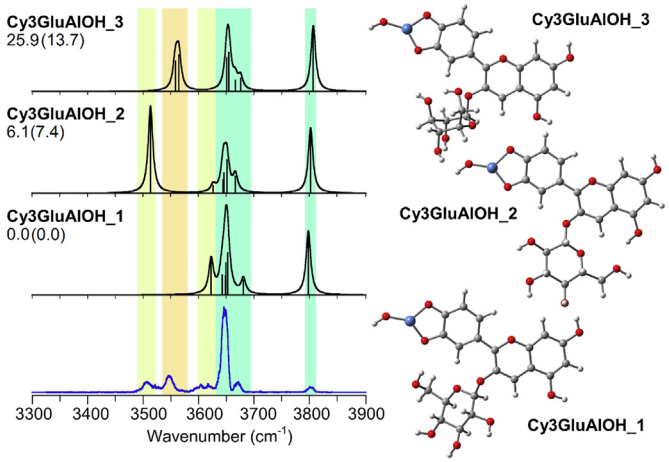

Fig. 9. IRMPD spectrum of $[(Cy3Glu\text{-}2H)AlOH]^+$ (blue profile) compared with IR spectra (B3LYP/6-311 + G** level) for conformers **Cy3GluOH_1**, **Cy3GluAlOH_2** and **Cy3GluAlOH_3** (black profiles), whose structures are reported on the right. Relative $\Delta G°(298\ K)$ calculated at the B3LYP and B3LYP-D3 (in brackets) level are reported in kJ mol^{-1}. (For interpretation of the references to color in this figure legend, the reader is referred to the Web version of this article.)

which aluminum is coordinated to the deprotonated hydroxyl groups in C6" and C3'. However, the comparison of the calculated spectra with the experimental one rather disproves the presence of **AlOHCy3Glu_1** in the sampled ion population. In particular, the expected absorption at 3781 cm^{-1} associated to the AlO—H stretching, is not observed in the experimental spectrum. The same vibrational mode is calculated for **Cy3GluAlOH_1**, **Cy3GluAlOH_2** and **Cy3GluAlOH_3** at 3798, 3807 and 3800 cm^{-1}, respectively, in good agreement with the experiment at 3802 cm^{-1}. There is, however, once again a serious discrepancy in the intensity of this band between calculated IR and experimental IRMPD spectra.

As reported in Fig. 9, **Cy3GluAlOH_1**, **Cy3GluAlOH_2** and **Cy3GluAlOH_3** present the same skeletal arrangement as the calculated geometries for $\mathbf{Cy3Glu}^+$ with matching numbering. However, **Cy3GluAlOH_1** and **Cy3GluAlOH_3** differ from the respective $Cy3Glu^+$ homologues for the H-bond between sugar and ring B due the deprotonation of the aromatic hydroxyl group coordinated to aluminum. **Cy3GluAlOH_1** and **Cy3GluAlOH_3** present C6"OH···O(Al)C3′ and C3"OH···O(Al)C3′ hydrogen bond interactions, respectively. A detailed assignment of IRMPD features for $[(Cy3Glu\text{-}2H)AlOH]^+$ on the basis of calculated vibrational frequencies of **Cy3GluAlOH_1**, **Cy3GluAlOH_2** and **Cy3GluAlOH_3** is reported in Table S2 of the SD.

Focusing on the 3450 and 3630 cm^{-1} spectral range, the IRMPD spectrum presents three bands at 3621, 3543 and 3506 cm^{-1}. The absorption at 3621 cm^{-1} is in agreement with the calculated the C6"OH stretching mode involved in the hydrogen bond with O(Al) C3′ in **Cy3GluAlOH_1** calculated at 3623 cm^{-1}. The calculated spectrum of **Cy3GluAlOH_3** shows two vibrational modes at 3565 and 3559 cm^{-1}, that are consistent with the experimental band at 3543 cm^{-1}, due to the stretching vibrations of C2"O—H and C6"O—H, respectively. The experimental feature at 3506 cm^{-1} can be attributed to the C5O—H stretching mode hydrogen bonded to O(H)C6″ in **Cy3GluAlOH_2** and calculated at 3513 cm^{-1}. Also these latter modes are severely under represented in terms of intensity in the experimental spectrum relative to the exceptionally active band at 3645 cm^{-1}.

The IRMPD spectrum of $[(Cy3Gal\text{-}2H)AlOH]^+$ is reported in Fig. 10 (red profile), together with the calculated IR spectra (black profiles), while frequency values are listed together with attributed

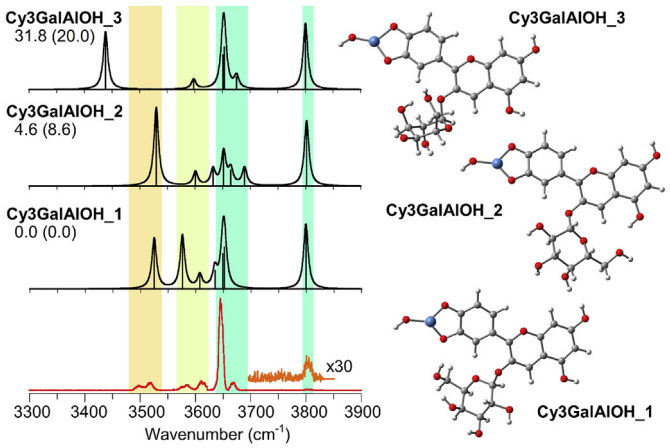

Fig. 10. IRMPD spectrum of $[(Cy3Gal\text{-}2H)AlOH]^+$ (red profile) compared with IR spectra (B3LYP/6-311 + G** level) for the conformers **Cy3GalAlOH_1**, **Cy3GalAlOH_2** and **Cy3GalAlOH_3**, whose structures are reported on the right. Relative $\Delta G°(298\ K)$ calculated at the B3LYP and B3LYP-D3 (in brackets) level are in kJ mol^{-1}. (For interpretation of the references to color in this figure legend, the reader is referred to the Web version of this article.)

vibrational modes in Table S3 in the SD. Geometries and calculated IR spectra of optimized conformers at higher energy are reported in Fig. S10. The interpretation of the $[(Cy3Gal\text{-}2H)AlOH]^+$ spectrum through calculations confirms the predominant chelation of aluminum through the deprotonated catechol hydroxyl groups. As observed in the case of the glucose counterpart, the presence of **Cy3GalAlOH_1**, **Cy3GalAlOH_2** and **Cy3GalAlOH_3**, showing (HO)Al binding to the deprotonated hydroxyl groups in C3′ and C4', may be confirmed by the experimental feature at 3802 cm^{-1}, in correspondence with calculated AlO—H stretching modes at 3800, 3802 and 3800 cm^{-1}, respectively. The intensity of the experimental band is once again exceedingly low. In analogy with the glucoside, an isomeric **AlOHCy3Gal_1**, is found to be the most stable species with a relative free energy of −21.1 kJ mol^{-1}. It presents, however, the same vibrational mode at 3782 cm^{-1} that is not detected in the IRMPD spectrum (Fig. S10 in the SD).

Moving to the informative 3400-3630 cm^{-1} range, it possible to exclude a significant contribution of **Cy3GalAlOH_3** in the assayed ionic population, due to the missing band expected at 3438 cm^{-1} (attributed to the C3"O—H stretching mode hydrogen bonded to O(H)C6″, see Table S3), although this mode could be poorly IRMPD active due to the above mentioned reason. This finding is in agreement with the supposed lower percentage of the $^1C_4$ conformation within galactosides with respect to glucosides (see sections 3.1.2 and ref [70—72]) and it is also confirmed by the higher relative free energy of **Cy3GalAlOH_3** compared to **Cy3GalAlOH_1** (at 31.8 and 20.0 kJ mol^{-1} at B3LYP and B3LYP-D3, respectively). A specific vibrational feature also discriminating the spectra of the two epimers is the absorption at 3583 cm^{-1}. It is found in the IRMPD spectrum of $[(Cy3Gal\text{-}2H)AlOH]^+$ and can be assigned to the C6"O—H stretching mode involved in the hydrogen bond with O(Al)C3′ of **Cy3GalAlOH_1**, expected at 3576 cm^{-1}. This absorption appears red-shifted with respect to the corresponding mode at 3621 cm^{-1} for **Cy3GluAlOH_1** (at 3621 cm^{-1} in the experiment) due to the combined involvement of the C6″OH group in a H-bond network, C4"OH··· (C6″)O - H ···O(Al)C3'. This pattern is, in fact, not allowed in the case of the glucoside.

4. Conclusions

A combined IM-MS, CID and IRMPD spectroscopy approach was used to discriminate among two epimeric compounds namely cyanidin 3-O-glucoside and cyanidin 3-O-galactoside, known to be abundant in red fruits. Results obtained with CID, IM-MS and IRMPD spectroscopy in the OH stretching range appear to be unsuccessful in distinguishing the two isomers. However, the IRMPD spectra of $Cy3Glu^+$ and $Cy3Gal^+$ in the fingerprint region have highlighted the presence of an absorption at 1080 cm^{-1} which is more significant in the $Cy3Glu^+$ isomer. The IRMPD spectrum of an ion at the same *m/z* 449 as the two standard compounds, delivered by ESI from a solution of pomegranate extract has presented this characteristic absorption, rather supporting the presence of cyanidin 3-O-glucoside in the sampled biological specimen.

Subsequently, inspired by what happens in nature (for example in *Hydrangea* plants) where the uptake of metal ions, such Al^{3+}, is responsible for the blue color of flowers, the interest turned towards the aluminum complexes of both epimers. IM-MS experiments on $[(Cy3Glu\text{-}3H)Al]^+$ and $[(Cy3Gal\text{-}3H)Al]^+$ have indicated that there are at least two different conformers for each species, displaying comparable mobility properties. More diagnostic information has been obtained by CID and IRMPD spectroscopy in the OH stretching range. The CID spectra show the presence of few characteristic fragment ions for each $[(Cy3Glu\text{-}2H)Al(OH)]^+$ and $[(Cy3Gal\text{-}2H)Al(OH)]^+$ species. IRMPD spectra in the OH stretching range display distinct bands at 3543 and at 3583 cm^{-1} which are peculiar to $[(Cy3Glu\text{-}2H)Al(OH)]^+$ and $[(Cy3Gal\text{-}2H)Al(OH)]^+$, respectively. A comparison with the computed IR spectra showed the aluminum ion to be coordinated through the deprotonated catechol moiety. Also, it was possible to attribute the differences observed in the experimental IRMPD spectra to specific structural features and to their influence on the preferred conformations of the two isomers. In particular, the presence of $^1C_4$ conformers in the gas-phase population of $[(Cy3Glu\text{-}2H)Al(OH)]^+$ has to be considered in order to interpret the experimental spectrum. Any contribution is instead negligible in the $[(Cy3Gal\text{-}2H)Al(OH)]^+$ epimer.

These results may pave the way for promising applications of IRMPD spectroscopy in the targeted characterization of anthocyanins in plants and fruits. The approach well integrates with high resolution FT-ICR-MS to reveal the full metabolic landscape, among which individual species may be selected for IR characterization.

Acknowledgements

This work has been supported by the Italian Ministry for Education, University and Research - Dipartimenti di Eccellenza - L. 232/2016, by the EU Horizon 2020 Programme under Grant Agreement No. 731077, by the French FT-ICR network (FR3624CNRS), and by the "e-ALIERB" Project (Regione Lazio LR13/2008 — Dipartimento di Chimica e Tecnologie del Farmaco). The authors wish to thank P. Maitre, D. Scuderi, J. M. Ortega and the CLIO team.

Appendix A. Supplementary data

Supplementary data to this article can be found online at https://doi.org/10.1016/j.ijms.2019.116179.

References

[1] G.A. Cooper-Driver, Contributions of Jeffrey Harborne and co-workers to the study of anthocyanins, Phytochemistry 56 (2001) 229—236, https://doi.org/10.1016/S0031-9422(00)00455-6.
[2] D. Strack, V. Wray, The anthocyanins, in: J.B. Harborne (Ed.), The Flavonoids Advances in Research since 1986, Chapman & Hall, London, 1994, pp. 1—22.
[3] T.M. Parkinson, J.P. Brown, Metabolic fate of food colorants, Annu. Rev. Nutr. 1 (1981) 175—205, https://doi.org/10.1146/annurev.nu.01.070181.001135.
[4] C.M. Ford, P.K. Boss, P. Bordier Høj, Cloning and characterization of *Vitis vinifera* UDP-glucose: flavonoid 3-O-glucosyltransferase, a homologue of the

enzyme encoded by the maize *Bronze*-1locus that may primarily serve to glucosylate anthocyanidins *in Vivo*, J. Biol. Chem. 273 (1998) 9224–9233, https://doi.org/10.1074/jbc.273.15.9224.
[5] F. Pina, Chemical applications of anthocyanins and related compounds. A source of bioinspiration, J. Agric. Food Chem. 62 (2014) 6885–6897, https://doi.org/10.1021/jf404869m.
[6] F. Pina, P. Vesselin, C.A.T. Laia, Photochromism of flavylium systems. An overview of a versatile multistate system, Dye. Pigm. 92 (2012) 877–889, https://doi.org/10.1016/j.dyepig.2011.03.033.
[7] M. Horbowicz, R. Kosson, A. Grzesiuk, H. Dębski, Anthocyanins of fruits and vegetables - their occurrence, analysis and role in human nutrition, crop, Res. Bull. 68 (2008) 5–22, https://doi.org/10.2478/v10032-008-0001-8.
[8] X. Ge, I. Timrov, S. Binnie, A. Biancardi, A. Calzolari, S. Baroni, Accurate and inexpensive prediction of the color optical properties of anthocyanins in solution, J. Phys. Chem. A 119 (2015) 3816–3822, https://doi.org/10.1021/acs.jpca.5b01272.
[9] K. Sakata, N. Saito, T. Honda, Ab initio study of molecular structure and excited states in anthocyanidins, Tetrahedron 62 (2006) 3721–3731, https://doi.org/10.1016/j.tet.2006.01.081.
[10] S. Masaaki, M. Naohiro, T. Kosaku, Structure of the blue cornflower pigment, Nature 436 (7052) (2005) 791, https://doi.org/10.1038/436791a.
[11] L. Cabrita, T. Fossen, Ø.M. Andersen, Colour and stability of the six common anthocyanidin 3-glucosides in aqueous solutions, Food Chem. 68 (1) (2000) 101–107, https://doi.org/10.1016/S0308-8146(99)00170-3.
[12] R.L. Jackman, R.Y. Yada, M.A. Tung, R.A. Speers, Anthocyanins as food colorants, J. Food Biochem. 11 (1987) 201–247, https://doi.org/10.1111/j.1745-4514.1987.tb00123.x.
[13] M.G. Miguel, Anthocyanins: antioxidant and/or anti-inflammatory activities, J. Appl. Pharm. Sci. 01 (06) (2011) 07–15.
[14] L.S. Einbond, K.A. Reynertson, X.D. Luo, M.J. Basile, E. Kennelly, Anthocyanin antioxidants from edible fruits, J. Food Chem. 84 (2004) 23–28, https://doi.org/10.1016/S0308-8146(03)00162-6.
[15] J.C. Espin, C. Soler-Rivas, H.J. Wichers, C. Garcia-Viguera, Anthocyanin-based natural colorants: a new source of antiradical activity for foodstuff, J. Agric. Food Chem. 48 (2000) 1588–1592, https://doi.org/10.1021/jf9911390.
[16] S.N. Nichenametla, T.G. Taruscio, D.L. Barney, J.H. Exon, A Review of the effects and mechanisms of polyphenolics in cancer, Crit. Rev. Food Sci. Nutr. 46 (2006) 161–183, https://doi.org/10.1080/10408390591000541.
[17] D.R. Bell, K. Gochenaur, Direct vasoactive and vasoprotective properties of anthocyanin-rich extracts, J. Appl. Physiol. 100 (2006) 1164–1170, https://doi.org/10.1152/japplphysiol.00626.2005.
[18] M.A. Lila, Anthocyanins and human health: an in vitro investigative approach, J. Biomed. Biotechnol. 2004 (2004) 306–313, https://doi.org/10.1155/S111072430440401X.
[19] S. Zafra-Stone, T. Yasmin, M. Bagchi, A. Chatterjee, J.A. Vinson, D. Bagchi, Berry anthocyanins as novel antioxidants in human health and disease prevention, Mol. Nutr. Food Res. 51 (2007) 675–683, https://doi.org/10.1002/mnfr.200700002.
[20] L. Ziberna, F. Tramer, S. Moze, U. Vrhovsek, F. Mattivi, S. Passamonti, Transport and bioactivity of cyanidin 3-glucoside into the vascular endothelium, Free Radic. Biol. Med. 52 (2012) 1750–1759, 10.1016%2Fj.freeradbiomed.2012.02.027.
[21] F. Galvano, L. La Fauci, G. Lazzarino, V. Fogliano, A. Ritieni, S. Ciappellano, N.C. Battistini, B. Tavazzi, G. Galvano, Cyanidins: metabolism and biological properties, J. Nutr. Biochem. 15 (2004) 2–11, https://doi.org/10.1016/j.jnutbio.2003.07.004.
[22] T. Fossen, O.M. Andersen, Spectroscopic techniques applied to flavonoids, in: O. M Andersen, K. Rr Markham (Eds.), Flavonoids—Chemistry, Biochemistry and Applications, Taylor & Francis, USA, 2005, pp. 37–142, https://doi.org/10.1201/9781420039443.ch2.
[23] J.S. Barnes, K.A. Schug, Structural characterization of cyanidin-3,5-diglucoside and pelargonidin-3,5-diglucoside anthocyanins: multi-dimensional fragmentation pathways using high performance liquid chromatography-electrospray ionization-ion trap-time of flight mass spectrometry, Int. J. Mass Spectrom. 308 (2011) 71–80, https://doi.org/10.1016/j.ijms.2011.07.026.
[24] M.C. Oliveira, P. Esperanc, M.A. Almoster Ferreira, Characterisation of anthocyanidins by electrospray ionisation and collision-induced dissociation tandem mass spectrometry, Rapid Commun. Mass Spectrom. 15 (2001) 1525–1532, https://doi.org/10.1002/rcm.400.
[25] Q. Tian, M.M. Giusti, G.D. Stoner, S.J. Schwartz, Screening for anthocyanins using high-performance liquid chromatography coupled to ESI tandem MS with precursor-ion analysis, product-ion analysis, common-neutral-loss analysis, and selected reaction monitoring, J. Chromatogr. A 1091 (2005) 72–82, https://doi.org/10.1016/j.chroma.2005.07.036.
[26] L. Hartmanova, V. Ranc, B. Papouskova, P. Bednar, V. Havlicek, K. Lemr, Fast profiling of anthocyanins in wine by desorption nano-ESI mass spectrometry, J. Chromatogr. A 1217 (2010) 4223–4228, https://doi.org/10.1016/j.chroma.2010.03.018.
[27] V. Vukics, A. Guttman, Structural characterization of flavonoid glycosides by multi-stage mass spectrometry, Mass Spectrom. Rev. 29 (2010) 1–16, https://doi.org/10.1002/mas.20212.
[28] B.D. Davis, P.W. Needs, P.A. Kroon, J.S. Brodbelt, Identification of isomeric flavonoid glucuronides in urine and plasma by metal complexation and LC-ESI-MS/MS, J. Mass Spectrom. 41 (2006) 911–920, https://doi.org/10.1002/jms.1050.
[29] J. Zhang, J. Wang, J.S. Brodbelt, Characterization of flavonoids by aluminum complexation and collisionally activated dissociation, J. Mass Spectrom. 40 (2005) 350–363, https://doi.org/10.1002/jms.793.
[30] S.A. Robotham, J.S. Brodbelt, Identification of flavone glucuronide isomers by metal complexation and tandem mass spectrometry: regioselectivity of uridine 5'-diphosphate-glucuronosyltransferase isozymes in the biotransformation of flavones, J. Agric. Food Chem. 61 (2013) 1457–1463, https://doi.org/10.1021/jf304853j.
[31] R. March, J. Brodbelt, Analysis of flavonoids: tandem mass spectrometry, computational methods, and NMR, J. Mass Spectrom. 43 (2008) 1581–1617, https://doi.org/10.1002/jms.1480.
[32] M.E. Crestoni, B. Chiavarino, D. Scuderi, A. Di Marzio, S. Fornarini, Discrimination of 4-hydroxyproline diastereomers by vibrational spectroscopy of the gaseous protonated species, J. Phys. Chem. B 116 (2012) 8771–8779, https://doi.org/10.1021/jp302382p.
[33] D. Scuderi, E. Bodo, B. Chiavarino, S. Fornarini, M.E. Crestoni, Amino acid oxidation: a combined study of cysteine oxo forms by IRMPD spectroscopy and simulations, Chem. Eur J. 22 (2016) 17239–17250, https://doi.org/10.1002/chem.201603298.
[34] B. Gregori, L. Guidoni, M.E. Crestoni, P. de Oliveira, C. Houée-Levin, D. Scuderi, One-electron oxidation of methionine-containing dipeptides of reverse sequence: sulfur versus sulfoxide characterized by IRMPD spectroscopy and static and dynamics DFT simulations, J. Phys. Chem. B 121 (2017) 2083–2094, https://doi.org/10.1021/acs.jpcb.6b12638.
[35] D. Corinti, B. Gregori, L. Guidoni, D. Scuderi, T.B. McMahon, B. Chiavarino, S. Fornarini, M.E. Crestoni, Complexation of halide ions to tyrosine: role of non-covalent interactions evidenced by IRMPD Spectroscopy, Phys. Chem. Chem. Phys. 20 (2018) 4429–4441, https://doi.org/10.1039/c7cp06657k.
[36] D. Corinti, C. Coletti, N. Re, S. Piccirillo, M. Giampà, M.E. Crestoni, S. Fornarini, Hydrolysis of cis- and transplatin: structure and reactivity of the aqua complexes in a solvent free environment, RSC Adv. 7 (2017) 15877–15884, https://doi.org/10.1039/C7RA01182B.
[37] D. Corinti, A. De Petris, C. Coletti, N. Re, B. Chiavarino, M.E. Crestoni, S. Fornarini, Cisplatin primary complex with L-histidine target revealed by IR multiple photon dissociation (IRMPD) spectroscopy, ChemPhysChem 18 (2017) 318–325, https://doi.org/10.1002/cphc.201601172.
[38] J. Martens, V. Koppen, G. Berden, F. Cuyckens, J. Oomens, Combined liquid chromatography-infrared ion spectroscopy for identification of regioisomeric drug metabolites, Anal. Chem. 89 (2017) 4359–4362, https://doi.org/10.1021/acs.analchem.7b00577.
[39] J. Martens, G. Berden, H. Bentlage, K.L.M. Coene, U.F. Engelke, D. Wishart, M. van Scherpenzeel, L.A.J. Kluijtmans, R.A. Wevers, J. Oomens, Unraveling the unknown areas of the human metabolome: the role of infrared ion spectroscopy, J. Inherit. Metab. Dis. 41 (2018) 367–377, https://doi.org/10.1007/s10545-018-0161-8.
[40] A.P. Cismesia, M.R. Bell, L.F. Tesler, M. Alves, N.C. Polfer, Infrared ion spectroscopy: an analytical tool for the study of metabolites, Analyst 143 (2018) 1615–1623, https://doi.org/10.1039/c8an00087e.
[41] N.C. Polfer, J.J. Valle, D.T. Moore, J. Oomens, J.R. Eyler, B. Bendiak, Differentiation of isomers by wavelength-tunable infrared multiple-photon dissociation-mass spectrometry: application to glucose-containing disaccharides, Anal. Chem. 78 (2006) 670–679, https://doi.org/10.1021/ac0519458.
[42] B. Schindler, L. Barnes, G. Renois, C. Gray, S. Chambert, S. Fort, S. Flitsch, C. Loison, A.-R. Allouche, I. Compagnon, Anomeric memory of the glycosidic bond upon fragmentation and its consequences for carbohydrate sequencing, Nat. Commun. 8 (2017) 973, https://doi.org/10.1038/s41467-017-01179-y.
[43] H. Elferink, M.E. Severijnen, J. Martens, R.A. Mensink, G. Berden, J. Oomens, F.P.J.T. Rutjes, A.M. Rijs, T.J. Boltje, Direct experimental characterization of glycosyl cations by infrared ion spectroscopy, J. Am. Chem. Soc. 140 (2018) 6034–6038, https://doi.org/10.1021/jacs.8b01236.
[44] B. Chiavarino, M.E. Crestoni, S. Fornarini, S. Taioli, I. Mancini, P. Tosi, Infrared spectroscopy of copper-resveratrol complexes: a joint experimental and theoretical study, J. Chem. Phys. 137 (2012), 024307, https://doi.org/10.1063/1.4732583.
[45] O. Kurka, J. Roithová, P. Bednář, Examination of small molecule losses in 5-methylpyranopelargonidin MS/MS CID spectra by DFT calculations, J. Mass Spectrom. 49 (2014) 1314–1321, https://doi.org/10.1002/jms.3466.
[46] D. Corinti, L. Mannina, B. Chiavarino, V. Steinmetz, S. Fornarini, M.E. Crestoni, IRMPD signature of protonated pantothenic acid, an ubiquitous nutrient, Chem. Phys. Lett. 646 (2016) 162–167, https://doi.org/10.1016/j.cplett.2016.01.032.
[47] K. Lincke, J. Langeland, A.Ø. Madsen, H.V. Kiefer, L. Skov, E. Gruber, K.V. Mikkelsen, L.H. Andersen, M.B. Nielsen, Elucidation of the intrinsic optical properties of hydrogen-bonded and protonated flavin chromophores by photodissociation action spectroscopy, Phys. Chem. Chem. Phys. 20 (2018) 28678, https://doi.org/10.1039/C8CP05368E.
[48] D. Corinti, A. Maccelli, B. Chiavarino, P. Maitre, D. Scuderi, E. Bodo, S. Fornarini, M.E. Crestoni, Vibrational signatures of curcumin's chelation in copper(II) complexes: an appraisal by IRMPD spectroscopy, J. Chem. Phys. 150 (2019), 165101. https://doi.org/10.1063/1.5086666.
[49] J.C. Molano-Arevalo, W. Gonzalez, K. Jeanne Dit Fouque, J. Miksovska, P. Maitre, F. Fernandez-Lima, Insights from ion mobility-mass spectrometry, infrared spectroscopy, and molecular dynamics simulations on nicotinamide adenine dinucleotide structural dynamics: NAD^+ *vs.* NADH, Phys. Chem. Chem. Phys. 20 (2018) 7043–7052, https://doi.org/10.1039/C7CP05602H.

[50] J. Oliveira, N.F. Brás, M. Alhinho da Silva, N. Mateus, A.J. Parola, V. de Freitas, Grape anthocyanin oligomerization: a putative mechanism for red color stabilization? Phytochemistry 105 (2014) 178–185, https://doi.org/10.1016/j.phytochem.2014.05.006.

[51] D.P. Smith, T.W. Knapman, I. Campuzano, R.W. Malham, J.T. Berryman, S.E. Radford, A.E. Ashcroft, Deciphering drift time measurements from traveling wave ion mobility spectrometry-mass spectrometry studies, Eur. J. Mass Spectrom. 15 (2009) 113–130, https://doi.org/10.1255/ejms.947.

[52] J. Lemaire, P. Boissel, M. Heninger, G. Mauclaire, G. Bellec, H. Mestdagh, A. Simon, S. Le Caer, J.M. Ortega, F. Glotin, P. Maitre, Gas phase infrared spectroscopy of selectively prepared ions, Phys. Rev. Lett. 89 (2002) 273002, https://doi.org/10.1103/PhysRevLett.89.273002.

[53] J.M. Bakker, T. Besson, J. Lemaire, D. Scuderi, P. Maitre, Gas-phase structure of a π-allyl–palladium complex: efficient infrared spectroscopy in a 7 T Fourier transform mass spectrometer, J. Phys. Chem. A 111 (2007) 13415–13424, https://doi.org/10.1021/jp074935e.

[54] B. Chiavarino, M.E. Crestoni, S. Fornarini, D. Scuderi, J.-Y. Salpin, Interaction of cisplatin with adenine and guanine: a combined IRMPD, MS/MS, and theoretical study, J. Am. Chem. Soc. 135 (2013) 1445–1455, https://doi.org/10.1021/ja309857d.

[55] R.K. Sinha, P. Maitre, S. Piccirillo, B. Chiavarino, M.E. Crestoni, S. Fornarini, Cysteine radical cation: a distonic structure probed by gas phase IR spectroscopy, Phys. Chem. Chem. Phys. 12 (2010) 9794–9800. https://doi.org/10.1039/c003576a.

[56] A.P. Sobolev, L. Mannina, D. Capitani, G. Sanzò, C. Ingallina, B. Botta, S. Fornarini, M.E. Crestoni, B. Chiavarino, S. Carradori, M. Locatelli, A.M. Giusti, G. Simonetti, G. Vinci, R. Preti, C. Toniolo, M. Reverberi, M. Scarpari, A. Parroni, L. Abete, F. Natella, A. Di Sotto, A multi-methodological approach in the study of Italian PDO "Cornetto di Pontecorvo" red sweet pepper, Food Chem. 255 (2018) 120–131, https://doi.org/10.1016/j.foodchem.2018.02.050.

[57] M. Ferreiro-González, C. Carrera, A. Ruiz-Rodríguez, G.F. Barbero, J. Ayuso, M. Palma, C.G. Barroso, A new solid phase extraction for the determination of anthocyanins in grapes, Molecules 19 (2014) 21398–21410, https://doi.org/10.3390/molecules191221398.

[58] Z. Diaconeasa, D. Ruginǎ, C. Socaciu, High-Purity Anthocyanins isolation using solid phase extraction tehniques, Bull. Univ. Agric. Sci. Vet. Med. Cluj-Napoca. Food Sci. Technol. 73 (2016) 1–6, https://doi.org/10.15835/buasvmcn-fst:11986.

[59] S. Cesa, S. Carradori, G. Bellagamba, M. Locatelli, M.A. Casadei, A. Masci, P. Paolicelli, Evaluation of processing effects on anthocyanin content and colour modifications of blueberry (Vaccinium spp.) extracts: comparison between HPLC-DAD and CIELAB analyses, Food Chem. 232 (2017) 114–123, https://doi.org/10.1016/j.foodchem.2017.03.153.

[60] M.J. Frisch, G.W. Trucks, H.B. Schlegel, G.E. Scuseria, M.A. Robb, J.R. Cheeseman, G. Scalmani, V. Barone, B. Mennucci, G.A. Petersson, H. Nakatsuji, M. Caricato, X. Li, H.P. Hratchian, A.F. Izmaylov, J. Bloino, G. Zheng, J.L. Sonnenberg, M. Hada, M. Ehara, K. Toyota, R. Fukuda, J. Hasegawa, M. Ishida, T. Nakajima, Y. Honda, O. Kitao, H. Nakai, T. Vreven, J.A. Montgomery Jr., J.E. Peralta, F. Ogliaro, M. Bearpark, J.J. Heyd, E. Brothers, K.N. Kudin, V.N. Staroverov, R. Kobayashi, J. Normand, K. Raghavachari, A. Rendell, J.C. Burant, S.S. Iyengar, J. Tomasi, M. Cossi, N. Rega, J.M. Millam, M. Klene, J.E. Knox, J.B. Cross, V. Bakken, C. Adamo, J. Jaramillo, R. Gomperts, R.E. Stratmann, O. Yazyev, A.J. Austin, R. Cammi, C. Pomelli, J.W. Ochterski, R.L. Martin, K. Morokuma, V.G. Zakrzewski, G.A. Voth, P. Salvador, J.J. Dannenberg, S. Dapprich, A.D. Daniels, Ö. Farkas, J.B. Foresman, J.V. Ortiz, J. Cioslowski, D.J. Fox, Gaussian09, Revision D.01, Gaussian, Inc., Wallingford CT, 2009.

[61] C.T. Lee, W.T. Yang, R.G. Parr, Development of the Colle-Salvetti correlation-energy formula into a functional of the electron-density, Phys. Rev. B 37 (1988) 785–789, https://doi.org/10.1103/PhysRevB.37.785.

[62] A.D. Becke, Density-functional thermochemistry.3. The role of exact exchange, J. Chem. Phys. 98 (1993) 5648–5652, https://doi.org/10.1063/1.464913.

[63] S. Grimme, J. Antony, S. Ehrlich, H. Krieg, A consistent and accurate *ab initio* parametrization of density functional dispersion correction (DFT-D) for the 94 elements H-Pu, J. Chem. Phys. 132 (2010) 154104, https://doi.org/10.1063/1.3382344.

[64] D. Corinti, C. Coletti, N. Re, R. Paciotti, P. Maître, B. Chiavarino, M.E. Crestoni, S. Fornarini, Short-lived intermediates (encounter complexes) in cisplatin ligand exchange elucidated by infrared ion spectroscopy, Int. J. Mass Spectrom. 435 (2019) 7–17, https://doi.org/10.1016/j.ijms.2018.10.012.

[65] B. Chiavarino, M.E. Crestoni, S. Fornarini, D. Scuderi, J.-Y. Salpin, Interaction of Cisplatin with 5'-dGMP: a combined irmpd and theoretical study, Inorg. Chem. 54 (2015) 3513–3522, https://doi.org/10.1021/acs.inorgchem.5b00070.

[66] A. Masci, A. Coccia, E. Lendaro, L. Mosca, P. Paolicelli, S. Cesa, Evaluation of different extraction methods from pomegranate whole fruit or peels and the antioxidant and antiproliferative activity of the polyphenolic fraction, Food Chem. 202 (2016) 59–69, https://doi.org/10.1016/j.foodchem.2016.01.106.

[67] M. Russo, C. Fanali, G. Tripodo, P. Dugo, R. Muleo, L. Dugo, L. De Gara, L. Mondello, Analysis of phenolic compounds in different parts of pomegranate (*Punica granatum*) fruit by HPLC-PDA-ESI/MS and evaluation of their antioxidant activity: application to different Italian varieties, Anal. Bioanal. Chem. 410 (2018) 3507–3520, https://doi.org/10.1007/s00216-018-0854-8.

[68] H. Li, K. Giles, B. Bendiak, K. Kaplan, W.F. Siems, H.H. Hill, Resolving structural isomers of monosaccharide methyl glycosides using drift tube and traveling wave ion mobility mass spectrometry, Anal. Chem. 84 (2012) 3231–3239, https://doi.org/10.1021/ac203116a.

[69] O. Hernandez, S. Isenberg, V. Steinmetz, G.L. Glish, P. Maitre, Probing mobility-selected saccharide isomers: selective ion–molecule reactions and wavelength-specific IR activation, J. Phys. Chem. A 119 (2015) 6057–6064, https://doi.org/10.1021/jp511975f.

[70] Y. Tan, N. Zhao, J. Liu, P. Li, C.N. Stedwell, L. Yu, N.C. Polfer, Vibrational signatures of isomeric lithiated N-acetyl-D-hexosamines by gas-phase infrared multiple-photon dissociation (IRMPD) spectroscopy, J. Am. Soc. Mass Spectrom. 28 (2017) 539–550, https://doi.org/10.1007/s13361-016-1575-x.

[71] K.A. Jebber, K. Zhang, C.J. Cassady, A. Chung-Phillips, Ab initio and experimental studies on the protonation of glucose in the gas phase, J. Am. Chem. Soc. 118 (1996) 10515–10524, https://doi.org/10.1021/ja960427z.

[72] L. Barnes, B. Schindler, S. Chambert, A.R. Allouche, I. Compagnon, Conformational preferences of protonated N-acetylated hexosamines probed by infrared multiple photon dissociation (IRMPD) spectroscopy and ab initio calculations, Int. J. Mass Spectrom. 421 (2017) 116–123, https://doi.org/10.1016/j.ijms.2017.05.005.

[73] J. Oomens, B.G. Sartakov, G. Meijer, G. Von Helden, Gas-phase infrared multiple photon dissociation spectroscopy of mass-selected molecular ions, Int. J. Mass Spectrom. 254 (2006) 1–19, https://doi.org/10.1016/j.ijms.2006.05.009.

[74] F. Turecek, C.L. Moss, I. Pikalov, R. Pepin, K. Gulyuz, N.C. Polfer, M.F. Bush, J. Brown, J. Williams, K. Richardson, Gas-phase structures of phosphopeptide ions: a difficult case, Int. J. Mass Spectrom. 354 (2013) 249–256.

[75] T.I. Yacovitch, N. Heine, C. Brieger, T. Wende, C. Hock, D.M. Neumark, K.R. Asmis, Vibrational spectroscopy of bisulfate/sulfuric acid/water clusters: structure, stability, and infrared multiple-photon dissociation intensities, J. Phys. Chem. A 117 (2013) 7081–7090.

[76] B. Chiavarino, M.E. Crestoni, M. Schütz, A. Bouchet, S. Piccirillo, V. Steinmetz, O. Dopfer, S. Fornarini, Cation-π interactions in protonated phenylalkylamines, J. Phys. Chem. A 118 (2014) 7130–7138, https://doi.org/10.1021/jp505037n.

[77] C. Fraschetti, L. Guarcini, M. Speranza, A. Filippi, Intramolecular n-type proton/hydrogen network in basic structures of vitamin B6 investigated by IRMPD spectroscopy, Int. J. Mass Spectrom. 438 (2019) 148–156, https://doi.org/10.1016/j.ijms.2019.01.006.

[78] U.A. Fischer, R. Carle, D.R. Kammerer, Identification and quantification of phenolic compounds from pomegranate (Punica granatum L.) peel, mesocarp, aril and differently produced juices by HPLC-DAD–ESI/MS(n), Food Chem. 127 (2) (2011) 807–821, https://doi.org/10.1016/j.foodchem.2010.12.156.

[79] G.T. Sigurdson, M.M. Giusti, Bathochromic and hyperchromic effects of aluminum salt complexation by anthocyanins from edible sources for blue color development, J. Agric. Food Chem. 62 (2014) 6955–6965, https://doi.org/10.1021/jf405145r.

[80] M. Buchweitz, G. Gudi, R. Carle, D.R. Kammerer, H. Schulz, Systematic investigations of anthocyanin–metal interactions by Raman spectroscopy, J. Raman Spectrosc. 43 (2012) 2001–2007, https://doi.org/10.1002/jrs.4123.

[81] K. Oyama, T. Yamada, D. Ito, T. Kondo, K. Yoshida, Metal complex pigment involved in the blue sepal color development of hydrangea, J. Agric. Food Chem. 63 (2015) 7630–7635, https://doi.org/10.1021/acs.jafc.5b02368.